Nuclear Science and Techniques (2026) 37:66
https://doi.org/10.1007/s41365-026-01891-9

Development of a prototype dual-aperture dipole magnet for CEPC collider

Mei Yang[1] · Fu-San Chen[1,2] · Jian-Xin Zhou[1] · Ya-Feng Wu[1] · Ying-Shun Zhu[1,2] · Xian-Jing Sun[1] · Chuang Shen[1,3]

Received: 25 October 2024 / Revised: 4 January 2025 / Accepted: 10 April 2025 / Published online: 30 January 2026

Abstract
The Circular Electron Positron Collider (CEPC) proposed in China is a dual-ring collider with electron and positron beams in the energy range of 45.5–180 GeV. The main dipole in the CEPC collider is a dual-aperture dipole with a shared coil between the two apertures, forming an I-shaped structure that can reduce power consumption by 50%. Because of its long length and low field strength, the development of this dual-aperture magnet faces challenges regarding its mechanical design, field measurement accuracy, and field performance. Numerical simulations were performed to better understand the Earth's field and the effect of different BH curves on field performance. The field results of the prototype are presented herein, and the field quality satisfies the requirements. The remanent field accounts for 2% of the integral field at 140 Gs, and the hysteresis effect caused an increase in field strength of approximately 0.075% after a standardization cycle of the trim coils. Research on this prototype can provide useful insights for understanding low-field dipole magnets.

Keywords CEPC collider · Dual-aperture magnet · Magnet design · Field measurement · Earth field

1 Introduction

The planned Circular Electron Positron Collider (CEPC) is a collider with a circumference of 100 km in China. The accelerator device consists of a linear accelerator, damping ring, booster, collider, and several transport lines. The CEPC collider can function as a W, Z, Higgs, or ttbar factory, corresponding to beam energies of 45.5, 80, 120, and 180 GeV. The collider has a double-ring scheme and shares the same tunnel as the CEPC Booster [1–3].

According to the FODO lattice of the CEPC collider, there are more than 3100 dipole magnets, 4000 quadrupole magnets, 3000 sextupole magnets and 7000 correctors [4]. Both the field strength and gradient of the dipole and quadrupole magnets in the CEPC Collider are relatively low, so they are designed as warm iron-dominated magnets, except in the IR regions [5, 6]. With such a large-scale magnet system, we need to make unremitting efforts in magnet design, construction, and commissioning to ensure economical cost and sufficient magnetic field performance.

The electron and positron beams gain energy in the RF cavities and lose energy due to synchrotron radiation in the dipoles distributed along the collider circumference [7, 8]. Most synchrotron radiation is produced by arc-bending magnets. Because the beam energy is very high, the synchrotron radiation in arc dipoles has a significant effect on the beam behavior, leading to a substantial sawtooth shape variation in the central beam energy along the ring, which is called the energy sawtooth effect [9]. With only two RF stations, the sawtooth orbit in the CEPC rings is approximately 1 mm for Higgs running. Beams with an off-center orbit will encounter an additional field in the magnets, resulting in a 5% distortion of the beam optics and a reduction in dynamic aperture (DA). To compensate for the closed orbit and optical function distortion, the magnetic field strength in the two apertures should be tapered independently of the

✉ Mei Yang
yangmei@ihep.ac.cn

[1] Institute of High Energy Physics, Chinese Academy of Sciences, 19B Yuquan Road, Beijing 100049, China

[2] University of Chinese Academy of Sciences, Beijing 100049, China

[3] China Spallation Neutron Source, Institute of High Energy Physics, Chinese Academy of Sciences, 1 Zhongziyuan Road, Dongguan 523000, China

energy along the beam orbit in the collider [10, 11]. Therefore, the main dipole and quadrupole magnets are designed with trim coils to fine-tune the field strength and gradient by approximately ±1.5%.

As the CEPC beam energy increases, the radiated power, which is proportional to the fourth power of the energy, affects various accelerator components, including the vacuum chamber, magnet coils, and cables [9]. Lead blocks are used as a shield against synchrotron radiation [12–14].

The CEPC is planned to be built underground, and the tunnel cross section directly determines civil engineering costs. The electron and positron rings are compact and parallel in most regions. The main dipole and quadrupole magnets are designed as dual-aperture magnets for power and cost savings, as proposed by FCC-ee [15–18]. The total length of the dipole magnet was approximately 70 km. Because the dipole magnets were maintained as long as possible to limit synchrotron radiation losses, each dipole magnet had a length of approximately 28 m. The core was divided into several sections in the longitudinal direction for ease of fabrication and transport, similar to the design of LEP [19]. The cores of one magnet are installed end-to-end in groups, and the coils of different cores are connected in series to form a complete dipole magnet.

Due to the large perimeter of the CEPC collider and the strong synchrotron radiation effect, the dipole field is very low, and its uniformity will be affected by the residual field of the magnetic materials [20, 21]. The collider operates at four different energies; therefore, the field uniformity in the dipole magnet may vary depending on the permeability of the magnetic material. A full-scale prototype of a dual-aperture dipole magnet (DAD) with a magnetic length of 5.7 m was developed to verify the magnet design, field quality, and excitation characteristics. In the prototype measurement, the repeatability of the magnetic field excitation and the effect of residual magnetization caused by hysteresis on the magnetic field uniformity in a good magnetic field area should be observed, which is difficult to evaluate in numerical simulations.

2 Magnetic design and considerations

According to the CEPC Conceptual Design Report, the dipole magnet will operate at 4 different field strengths, covering the beam energy range from 45.5 GeV to 180 GeV. All magnets function in DC mode at one field strength at a time. The main dipole characteristics are listed in Table 1. The overall magnetic field strength is minimal; therefore, the magnet core operates at a very low field, corresponding to the initial segment of the magnetization curve, which is nonlinear.

Table 1 Main parameters of the CEPC collider ring dipole magnets

Parameters	Value
Field strength@45.5 GeV (Gs)	140
Field strength@180 GeV (Gs)	560
Gap height (mm)	70
Effective length (m)	28.7, 5 parts
Good-field region radius (mm)	13.5
Field quality	$\leq 5\times10^{-4}$
Trim coil adjustment capability	±1.5%
Center field difference in two apertures	≤0.5%

As an electron and positron collider, the dipole magnets in the two rings have the same polarity and nearly the same field strength. Initially, two separate C-shaped dipole magnets were placed together, as shown in Fig. 1a. The cross and dot marks indicate the inflow and outflow of the current in the excitation coils, which represent the negative and positive directions of the current. In a single-dipole magnet, an external current loop outside the iron core is essential as a closed loop; however, its contribution to the central magnetic field is negligible. Although the two parallel C-type dipole magnets have the same field strength, the current directions in the coils between the two yokes are opposite. When these two magnets are considered as a whole system, they can cancel each other out. The parallel magnets can then be placed closer together and simplified as dual-aperture dipole magnets, as shown in Fig. 1b. The coils inside the apertures are connected to a closed circuit. Compared to the two separate magnet placement schemes, the total lengths and areas of the coils were reduced by 50%, as was the power consumption. This I-shaped dual-aperture dipole magnet is the first option for the CEPC collider.

The beam separation between the two apertures is 350 mm, determined by the vacuum chamber, the synchrotron radiation shielding lead blocks, and the excitation coil [13]. Solid iron (DT4) was used for the yoke and poles to simplify the structure of the magnet. The iron core consists of three parts: the upper and lower poles and the center support yoke. The main coil is wound around the central yoke. The trim coils were wound around the upper and lower poles of the left and right apertures, respectively. Two small power sources were used to excite the trim coils in the two apertures for independent tapering. The lead blocks on both sides of the vacuum chamber ensured the resistance of the coils to synchrotron radiation. Stainless steel blocks are placed at intervals on the open sides of the two apertures. These support the poles and reduce the deformation of the magnetic poles.

For an iron-dominated magnet, its field quality strongly depends on the pole profile. The simplest parallel pole surfaces were chosen to reduce manufacturing costs. A

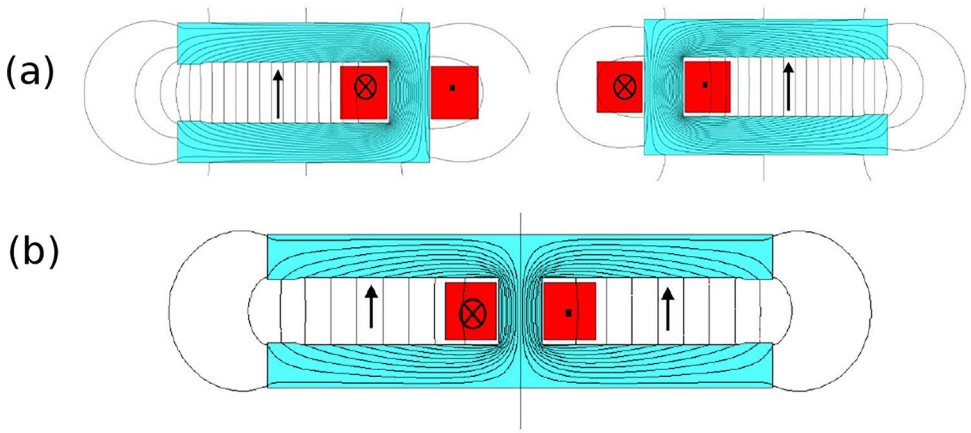

Fig. 1 (Color online) Two C-shaped dipole magnets placed side by side (**a**) and dual-aperture dipole magnet (**b**)

trapezoidal platform on the opening sides was used to improve field uniformity. Magnetic field simulations were performed using the FEA software OPERA [22]. The fields in the two apertures of the DAD were asymmetric. In the ideal DAD model, the structure is symmetrical about the central yoke; however, the opening gaps of the two holes are located on opposite sides. Therefore, the amplitudes of the high-order harmonics within the two apertures are the same; the signs of the odd-order harmonics are identical, but the signs of the even-order harmonics are opposite.

This DAD magnet has no obvious poles, and the field is very sensitive to the positions of the coils. This implies that the coils should be symmetrical with respect to the upper and lower poles. Field error analysis shows that with a 2 mm position error of the coil, a skew dipole term of 3.4×10^{-4} is introduced. Once there is a slope in the pole face, an error of 0.015 mm changes the field uniformity by 0.6×10^{-4}. This demonstrates the need for controlled tolerances in coil and pole-profile machining.

2.1 Influence of magnetic materials on magnetic field

Usually, the multipole component is expressed in "units," which means a strength of 0.01% or 100 ppm normalized to the fundamental field [23]. Here, the fundamental field is the normal dipole field in the DAD.

The general BH curve (DT4medium.bh) is used for the core material. The transverse distributions of B_y at different energies were simulated and are plotted in Fig. 2. At the first two working points of 45.5 GeV and 80 GeV, the field uniformity was nearly the same. At 120 GeV and 180 GeV, the distribution differed from that at the first two working points. The main difference was in the quadrupole component, with a maximum difference under the four energies of the two units.

Several previously measured BH curves were incorporated into the same model, which is plotted in Fig. 3a. The tenten.bh and default.bh curves are built-in curves of OPERA. There were slight changes in the magnetic field strength and significant differences in the magnetic field uniformity. The material with a higher permeability

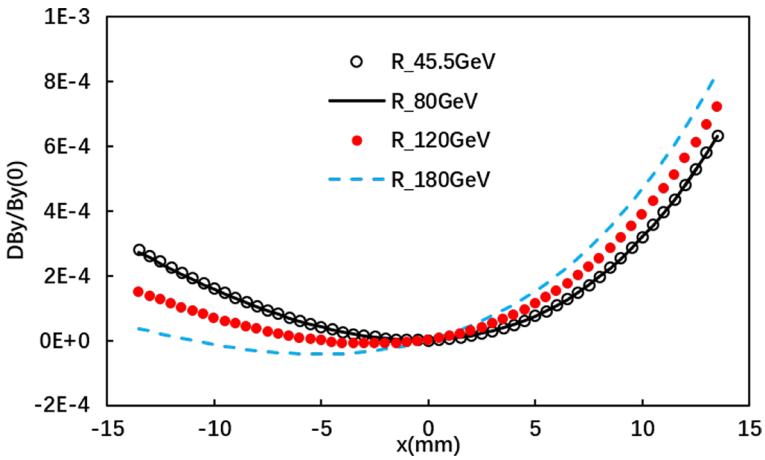

Fig. 2 (Color online) Transverse field distribution in the right aperture of DAD at different energies

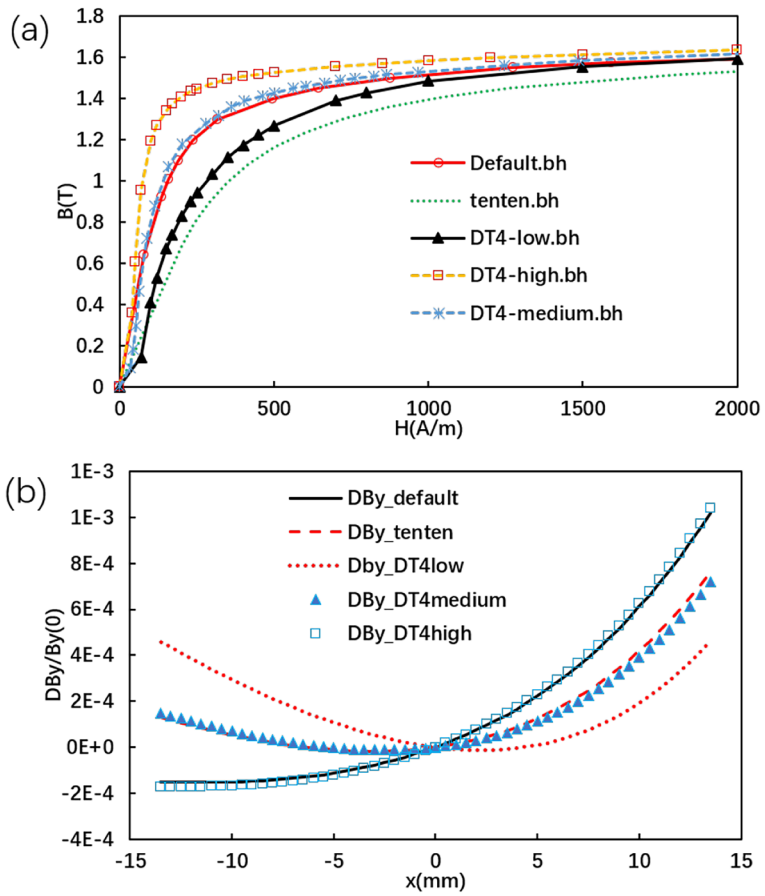

Fig. 3 (Color online) BH curves of different iron materials (**a**) and transverse distribution of B_y in DAD with different BH curves at 120 GeV (**b**)

(DT4high.bh) produced a higher magnetic field strength than the other materials (tenten.bh) by approximately 0.9%.

Figure 3b shows the field distribution in the right aperture at 120 GeV, when the central field B_y is approximately 373 Gs. Significant differences were observed in the transverse distribution of the magnetic field with different core materials. This indicates that variations in magnetic materials can affect the uniformity of the magnetic field and high-order harmonic components. The quadrupole component, which is the first higher-order component of a dipole magnet, is particularly sensitive to these changes. The initial phase of the BH curve also exhibited nonlinearity. Considering that the magnetic induction intensity at the center of the magnet spans approximately four times across the four operating points, even though the magnetic field strength of the magnet is low, the magnetic material demonstrates nonlinear behavior in the low-field region, which affects the uniformity of the magnetic field.

For tenten.bh and default.bh, the field distributions at the four field strengths are nearly identical. This is due to their BH curves being relatively smooth and linear in the operating region of the DAD magnet.

2.2 Effects of the Earth field propagation in the dipole aperture

In the CEPC collider, the DAD has a minimum field strength of 140 Gs and a field uniformity requirement of 0.05%. Although the Earth's field is approximately 0.5 Gs and accounts for 0.3% of the lowest field, its propagation varies with different orientations of the device or the main field direction. Several studies have been conducted on ID devices and low-field dipole magnets [24, 25]. Therefore, the influence of Earth's magnetic field on the magnetic performance of DAD in different orientations must be evaluated.

A pair of parallel current plates is used to approximate the distribution of the Earth's magnetic field and to simulate its propagation through the aperture and iron of DAD. The first simulation without DAD iron was performed to define Earth's field value in the model region. The distribution of the Earth's field in the DAD region is close to constant. For the Earth field in one direction, the same finite element model was used for all simulation cases, differing only in the material settings of the coils and iron core.

Both the horizontal and vertical Earth fields are considered, and the flux line distribution in DAD is shown in

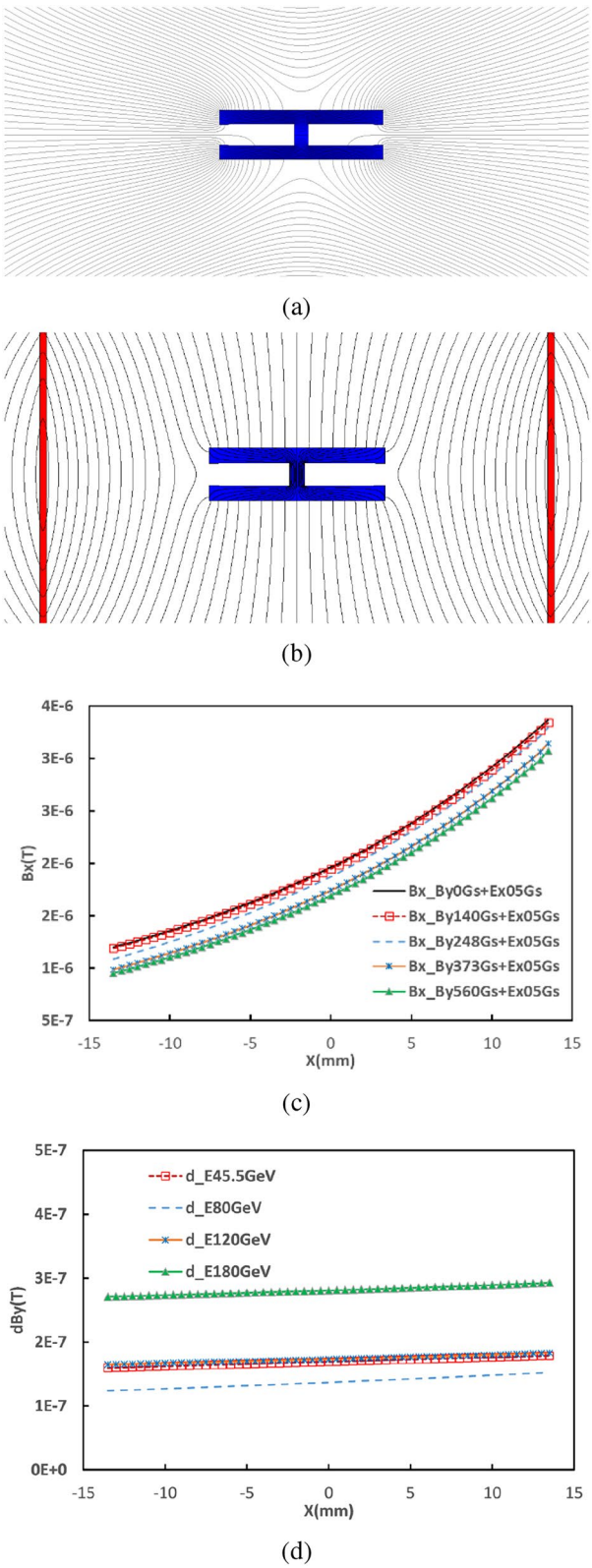

Fig. 4 (Color online) Flux lines in DAD with **a** horizontal and **b** vertical Earth fields only, **c** introduced B_x by horizontal Earth field in different cases, and **d** introduced B_y by vertical Earth field in different cases

Fig. 4a and b. The magnetic flux is bent and concentrated through the iron core because its magnetic resistance is much lower than that of air. However, there remains a leakage field that propagates through the two apertures of the magnet, which is our concern.

With no exciting current in the DAD, the horizontal Earth field, which is perpendicular to the main field B_y, introduces a horizontal field B_x of approximately 0.02 Gs in the gap of the apertures, and the variations of B_x in the good-field region are less than 0.015 Gs. No vertical component B_y exists in the two apertures. The main dipole field is in the vertical direction, and its magnitude and distribution remain almost unchanged. When the field strength of the main field differs, the B_x component introduced by Earth's field within the good-field area varies slightly, as shown in Fig. 4c. The largest harmonic introduced by the horizontal Earth field is the skew dipole a_1, approximately 1.5 units at 140 Gs, which requires special attention. The introduced field B_x is almost the same for all cases. This effect is similar even when the main current is zero. Subsequently, the impact of the horizontal Earth field decreases with an increase in the main magnetic field.

If the Earth field is vertical, it will increase or decrease the main field in the Y direction. When the vertical Earth field is 0.5 Gs, the average field increment (dB_y) is approximately 0.0028 Gs, as shown in Fig. 4d, which is reduced by almost 1 order of magnitude compared to that in the horizontal Earth field. Magnetic poles shield the Earth's vertical field; therefore, the propagation of the vertical Earth field in DAD can be neglected.

2.3 3D field simulation of DAD

The 3D field simulation is also performed in OPERA/3D. The model was extruded from a 2D model, and its core length is 5.67 m. At a nominal operating current of 1063 A, the calculated magnetic field reaches 373 Gs, which corresponds to an energy of 120 GeV. At 1623 A, the central field is 560 Gs at 180 GeV and the power dissipation is approximately 1.3 kW.

The effective length is approximately 5.78 m. It is longer than the core length, and the increment is greater than 1.15 times the gap height, as supplied by the empirical formula $Leff = Liron + (1.05 \sim 1.15)\,\mathrm{Gap}$ [26]. This indicates that the low-field dipole has a larger effective length. In practice, an accurate effective length should consider nearby components, such as the neighboring magnet and end coil. The effective length of the DAD at different field strengths varies slightly, with a maximum difference of 1.4×10^{-4}. This can be compensated for by interpolating the excitation curve and adjusting the excitation current.

The integral field uniformity of B_y is somewhat different from the central field uniformity, especially in such a long

dipole magnet. The main reason for this is that the shared coil in the middle of the dual-aperture magnet is not symmetrical on either side of the good-field region of one aperture, which introduces an asymmetric field, such as a quadrupole field. The integral end field in the good-field region indicates that the field outside the iron has been integrated. The main harmonic components of the end-integral field are the quadrupole and sextupole components, with values of 106 and 36 units, respectively. This constitutes a small proportion of the total integral field (approximately 2%). This slightly alters the integral field; therefore, no end-field chamfer is required in this long magnet. The integral field harmonics at the four energies were calculated. The main difference in the harmonics at different field strengths is the quadrupole component, which is influenced by the end field and main coil. The other components were nearly identical to those in the 2D simulation. The trim coils had little effect on the field uniformity in both their aperture and other apertures.

3 Mechanical design and prototype manufacturing

The dual-aperture dipole mainly includes an iron core, supports, aluminum busbar coils, trim coils, and a cooling system. The iron core consists of three parts: the upper and lower poles, and the central yoke. The two poles are bolted to the central yoke with positioning pins at the top, bottom, and ends. The core length is 5670 mm, and the cross section measures 530 mm × 160 mm. The total weight of the prototype is approximately 2.6 tons. The central yoke has a width of 46 mm, compared to the pole width of 530 mm. Given the structure's large leverage due to the narrow yoke and wide poles, the flatness requirement for the central yoke is very stringent; otherwise, amplification errors can easily occur at the opening gap. Concurrently, spaced contour blocks made of stainless steel were added at the opening side to ensure consistent gap height and reduce the slope of the pole. Threaded holes were pre-drilled at each end of the magnet for end shimming, if required.

Based on numerical simulations and the general machining level, the total mechanical tolerance is ±50 μm, which includes profile and assembly errors. This tolerance is achievable for such long magnets and is not particularly harsh.

For the exciting coil, an aluminum busbar was chosen for its low weight and cost compared to the copper conductor. In this prototype, the rectangular busbars have dimensions of 60 mm × 27 mm. The total power dissipation of all the dipole magnets exceeds 13 MW; therefore, the conductors must be cooled. The conductors were extruded from the former with a 6-mm-diameter cooling hole. Several dipole magnets were connected in series with a voltage limit of approximately 1 kV. To reduce power consumption in the power cables, each magnet has two turns of busbar coils and end blocks that are connected in series with bolts and a sealing ring. Nitrogen gas at a pressure of 1 MPa is injected, and a sealing test is conducted. The aluminum busbars have a plasma-sprayed ceramic insulating coating on the surface with a thickness of 0.03 mm and are expected to withstand high voltages of up to 1000 V. The ceramic coating is an inorganic material sprayed onto the surface of a coil for electrical insulation and radiation resistance. Because aluminum is prone to oxidation, the contact surfaces are silver-plated or insulated and lacquered as required. The conducting contact surface is covered with a layer of indium flakes. Owing to indium's flexibility, excellent conductivity, and sealing properties, it effectively reduces contact resistance. The trim coils were directly wound on the poles using enameled aluminum wires because of the small number of turns. They were then secured to the iron core using internal and external blocks.

It is crucial to study the manufacturing technology during machining. The core parts are processed using a CNC machine with a machining tolerance of less than 10 μm. The total tolerance of the aperture gap was less than ±50 μm which was checked using a stop-and-go gauge. At the maximum magnetic field strength, the electromagnetic force between the poles in the aperture was approximately 1600 N, which was far less than the gravitational force and could be neglected. The maximum deformation caused by gravity of the DAD simulated in ANSYS [27] is approximately 17 μm, which is local and smaller than the mechanical tolerance and can be disregarded. A special truss fixture was used to lift the magnet and reduce deformation during lifting.

Before leaving the factory, the magnet's coils were subjected to a high voltage test of 1000 V, and the leakage current was very high. The thickness of the external insulation layer of the busbars is less than 0.03 mm, and the coating technology used is not very stable. The large surface area of aluminum with such a thin ceramic layer could have produced local defects that significantly impacted the insulation properties. Therefore, the external insulation layer of polyimide tape was half-stacked over the coil, which was then insulated to pass the 1000 V high voltage test. Further research is being conducted on the potential of other inorganic insulation measures for the electrical insulation and radiation resistance of coils.

4 Field measurement of DAD prototype and analysis

All magnets should be measured individually to determine their excitation characteristics and magnetic field performance. The Hall probe system is a general method used for

measuring dipole magnets [28–30]. However, this is inefficient for batch magnets; therefore, a rotating coil measurement system was developed [31]. The prototype DAD was measured using both the Hall probe and rotating coil measurement system.

4.1 Main field measurement without trim coils

Prior to the field measurement, some test preparations were required. Oxygen-free copper bars were used as a bridge between the power cables to the power supply and the magnetic busbars, and water cooling was monitored for flow and temperature rise. The maximum current of the magnet was 1623 A. During the first excitation, the contact surfaces of the extended copper-bar adapters were relatively hot, which was effectively addressed by applying indium sheets to the contact surfaces.

The Hall probe was installed on a motion guide bracket, which is placed on the surface of the lower pole. The trolley with the Hall probe was driven back and forth by a motor and positioned by adjusting the support structure. The straightness and height of the Hall probe were maintained during movement. The position of the Hall sensor is fed back by a laser at one end. The DAD with the Hall probe measurement system is shown in Fig. 5a.

By scanning the longitudinal field of B_y, the integral field and central field are obtained in the two apertures. The measured central field in aperture A was 378.558 Gs when the excitation current of the main coil was 1067 A, which corresponded to a beam energy of 120 GeV. The effective length of the dipole magnet in aperture A was 5.75 m. The integral field difference between the two apertures was less than 0.1%, which satisfied the requirements. The integral field measured using the Hall probe was used to calibrate the coefficient of the rotating coil.

As shown in Fig. 5b, the rotating coil magnetic field measurement system mainly consists of a rotating coil skeleton, a titanium alloy outer sleeve, a rotating motor and control system, an encoder, a coupling joint, a multi-axis movable platform, a data acquisition system, and an industrial control computer. The skeleton of the rotating coil is generally made of a nonmagnetic material, with G10 used here. Due to the difficulty of achieving a length of 5.7 m with a slender skeleton, segmented coils were selected. The overall length of the rotating coil is approximately 6.5 m, composed of four 1.2 m long coils and one 0.84 m short coil. Self-centering and self-tightening structures were adopted

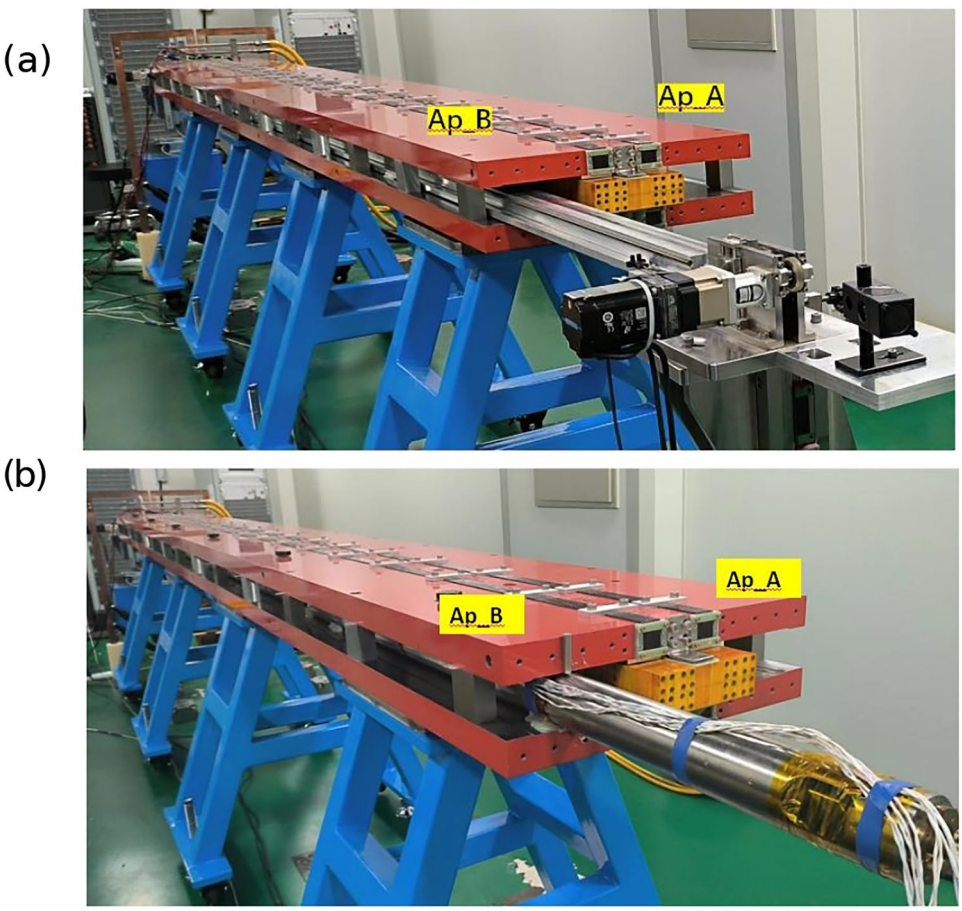

Fig. 5 (Color online) DAD magnet on the Hall probe measurement system (**a**) and on a rotating coil measurement system (**b**)

between the frame and outer tube. The adjacent subcoils were connected in series via a coupling and shaft. Auxiliary connection shaft holes were used to ensure that the coils were coaxial. Ceramic bearings are arranged at both ends of the coil. The connecting bolts and grooves are made of a nonmagnetic titanium alloy, which has minimal effect on the magnetic field.

Each coil has inner and outer coils wound on the G10 skeleton, resulting in coil coefficients that are sensitive to high-order harmonic signals. The signals from the subcoils are individually led out by nonmetallic slip rings. Each subcoil has a buckling scheme and should be individually calibrated. Different parts of the magnet can be measured and analyzed, particularly at the ends.

Generally, the radial and azimuthal components of a two-dimensional field in a current-free region (in the good-field region of the dipole magnet) can be expressed as below [32].

$$B_r(r,\theta) = B_N \sum_{n=1}^{\infty} [b_n(r)\sin(n\theta) + a_n(r)\cos(n\theta)], \tag{1}$$

$$B_\theta(r,\theta) = B_N \sum_{n=1}^{\infty} [b_n(r)\cos(n\theta) - a_n(r)\sin(n\theta)], \tag{2}$$

$$B_y = B_r \sin\theta + B_\theta cos\theta, \tag{3}$$

where b_n and a_n denote the normal and skew relative multipole coefficients related to the main field B_N, corresponding to the 2n-th normal and skew multipole components. R_{ref} denotes the reference radius; B_y is the vertical component in Cartesian coordinates and is generally used in a normal dipole magnet. The uniform distribution of the integral field versus x can be obtained using the formula:

$$\begin{aligned} \frac{\Delta B_y Leff}{B_y(x=0,y=0)Leff} &= \frac{B_y(x,y=0)Leff}{B_y(x=0,y=0)Leff} - 1 \\ &= \sum_{n=2}^{\infty} b_n \bar{x}^{n-1} \end{aligned} \tag{4}$$

In the above formula, $\bar{x}$ is the normalized horizontal axis and is equal to x/R_{ref}. b_n is the harmonic coefficient obtained using the rotating coil measurement system.

There are five rotating coils: coil 1 is located near the motor, followed by coils 2, 3, 4, and 5 in sequence. The magnetic coils are rotated within a magnetic field to obtain the induced voltage signals for each segment, which are accumulated to derive the integral field and multipole harmonics. The field uniformity can be determined through field harmonics, which can be calculated using formula (4) [33]. In Fig. 6a, the field uniformity of the five coils is plotted. The uniformities of the integral fields of the middle three coils are similar. The field uniformities of the first and last coils differ significantly from those in the middle section due to the end effect of the magnet.

The integration results of each coil are weighted and summed to obtain the integral field distribution in the good-field region of the entire magnet, as shown in Fig. 6b. Table 2 lists the high-order harmonics measured by the rotating coil measurement system within two apertures, with all high-order harmonic components being less than 4 units. The largest harmonic component of the integrated magnetic field measured at the two apertures was the sextupole component, which is consistent with the numerical simulation results (using DT4 high. bh). This result shows that the transverse integrated magnetic field distributions within the two apertures are almost identical, demonstrating good manufacturing tolerance in magnet processing.

The integral transfer function curves within the two apertures are compared. At the four working energies, the integral field differences between the two apertures were less than 0.1%, which satisfied the physical requirements. When the current decreased to 0, the measured remanent field occupied 1.5% of the integral field at 45.5 GeV, and the variation of remanence in the good-field region represented only 3×10^{-5} of the integral field at 45.5 GeV. In this prototype, the influence of the remanent field can be disregarded. In addition, the magnet was excited several times, and the integral field reproducibility was better than 6×10^{-5}, satisfying the physical requirements.

4.2 Magnetic field measurement with trim coils

We learned that during the ramping process, the trim coil interferes with the magnetic field strength generated by the existing main coil. Simultaneously, a hysteresis effect occurs during the excitation of the ferromagnetic materials. Different magnetic fields are generated if the ramp path of the trim coil changes. Therefore, it is necessary to follow a specific path when ramping the trim coil to ensure repeatability of the magnetic field excitation. The maximum current in the trim coils was 6 A during testing. The current in the main coil was 1067 A, which corresponded to a main field of 373 Gs. Following the general ramping process of the main coil, the trim coils ramped in the sequence of 0, 6 A, −6 A, 0 for three cycles. Magnetic field measurements were performed, and the excitation curve of the field induced by the trim coil is plotted in Fig. 7a. The linearity of the curve was very good. The tapered field at 6 A accounts for approximately 3.2% of the main field. The required correction amount of the dipole magnets at different longitudinal positions in the collider ring varies, and the trim coils' current can be adjusted as needed for each magnet. After the trim coil's current is loaded, the uniform distribution of the integrated

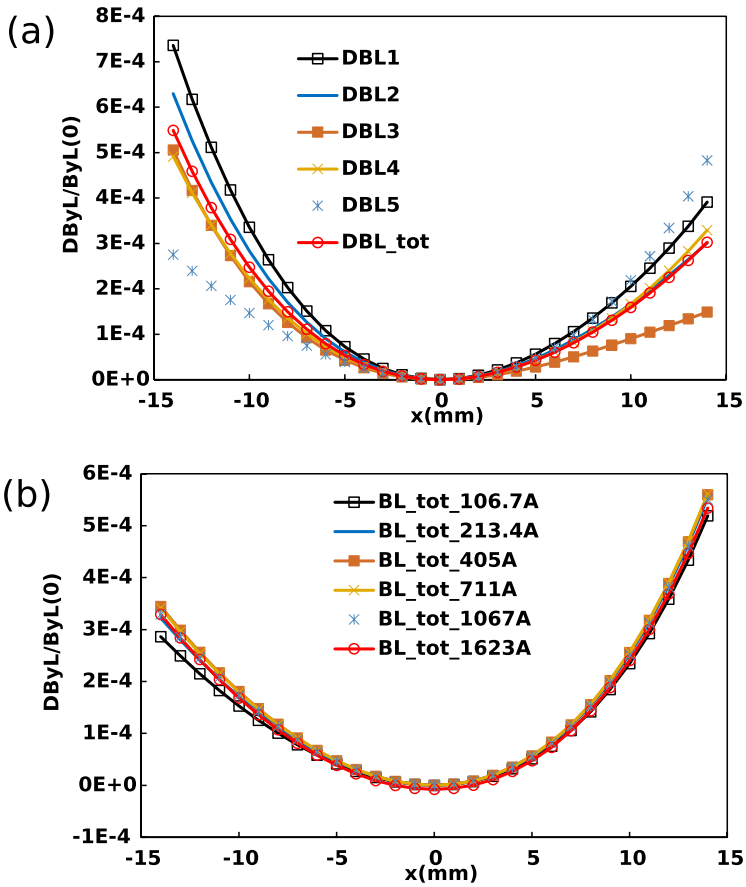

Fig. 6 (Color online) Uniformity distribution of the integrated field in 5 coils in aperture A @ 120 GeV (**a**) and uniformity distribution of integrated field under different currents in aperture A (**b**)

Table 2 Integral high-order harmonics in two apertures in DAD@120 GeV (units: 1×10^{-4})

n	b_n_L	b_n_R
2	0.01	0.01
3	3.92	3.88
4	1.03	−1.22
5	0.47	0.54

magnetic field of the dual-aperture dipole magnet remains unchanged.

When the trim coil in aperture A was standardized, the magnetic field in aperture B changed and showed an overall increase, as shown in Fig. 7b. During the coils' ramping process in aperture A from −6 to 6 A, the variation range of the field in aperture B was 4×10^{-4} ~10×10^{-4}, compared to the main integral field at 373 Gs. When the trim coil current in aperture A decreased to zero, the magnetic field increment ratio in aperture B was approximately 7.5×10^{-4}. Even if the current of the trim coil had the same value during the increase and decrease paths, the field strength differed, indicating that the hysteresis of the iron core affects the magnetic field.

Through experiments, it was found that after the current of the trim coil reduces to 0, the magnetic field repeats when the main coil is ramped up again, eliminating the influence of the trim coil's excitation on the magnetic field. This is called the wiping-out property of magnetic material [34–36]. When the main current reaches a certain value and the standardized loading path of the trim coil is the same, the influence of the trim coil on the main magnetic field is repeated. In practice, the trim coil can be cycled through a fixed standardized path, and current is applied to achieve the required magnetic field adjustment.

5 Summary

A prototype full-scale dual-aperture dipole magnet for the CEPC collider has been developed. The detailed design, machining process, and field measurement results are presented.

In the development, the precision achievable through the mechanical processing of the long prototype was emphasized, and the effects of different iron core materials (with varying BH curves) on the magnetic field excitation characteristics and quality of low-field dipole magnets were compared and analyzed. Because the yoke material significantly affects field uniformity, the entire yoke should be made from

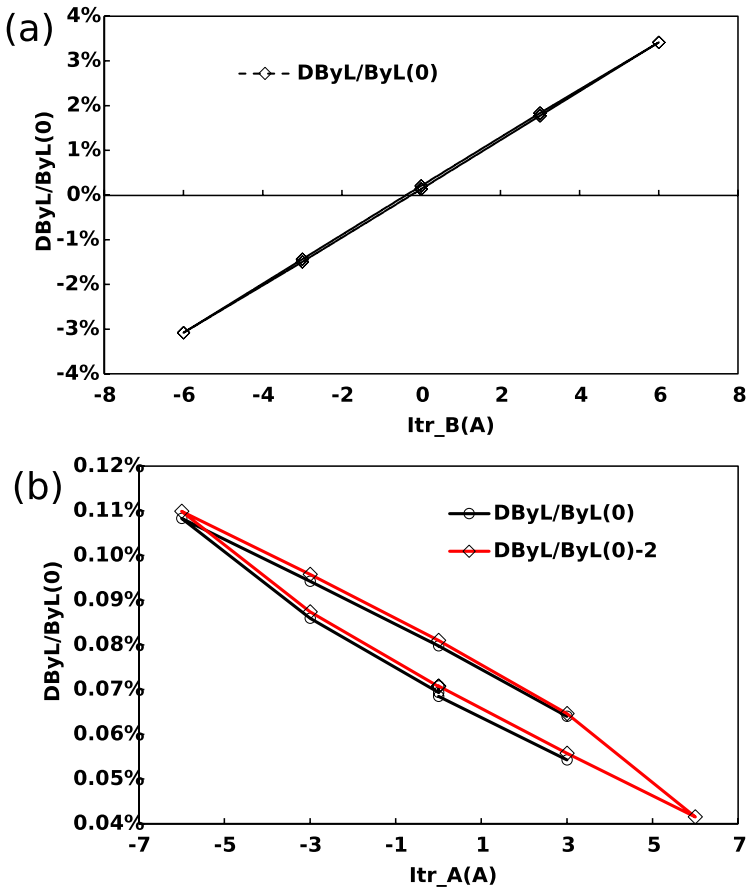

Fig. 7 (Color online) Proportion of magnetic field increased with trim coils (**a**) and influence of excited trim coils in aperture A on magnetic field in aperture B (**b**)

a single batch of material. In addition, other cost-effective magnetic materials, such as structural low-carbon steel, will be considered and studied later.

The prototype uses DT4, which has good magnetic properties, resulting in excellent linearity across different low magnetic field strengths. The transverse homogeneity of the integrated magnetic field was nearly identical for all four operating modes. This aligns with the simulation results for the DT4 high-BH curve, which demonstrates that the fabrication of magnets and the properties of the magnetic materials can satisfy these requirements. The trim coil of the dual-aperture dipole magnet fulfills the amplitude adjustment requirements and has minimal impact on the magnetic field distribution in the good-field region of the two apertures. The magnetic field regulation performance of the trim coil was studied through excitation experiments, and the field quality and reproducibility met the requirements at all field levels.

The successful development of this low-field dual-aperture prototype demonstrates the feasibility of achieving high field quality and 50% power savings. The stainless steel blocks at the opening gaps are used to ensure the gap height of the two apertures and maintain consistent field strength; other nonmagnetic materials are considered for use as support blocks. The aluminum busbar coils met the excitation requirements without significant overheating. Some technological choices, particularly regarding the coil conductor and yoke assembly, require further study to optimize the interfaces with several other systems (power, cooling and ventilation, and alignment). This prototype provides an effective reference for the development of collider dipole magnets.

Acknowledgements The authors would like to thank the Magnet Group of the Institute of High Energy Physics for their helpful comments on this research. We are also grateful to all the workshop members for providing invaluable suggestions on the mechanical design and manufacturing at Keye. Special thanks go to engineers Dapeng Yin and manager Xinlian Wu for their hard work.

Author contributions All authors contributed to the study conception and design. material preparation, data collection were performed by Mei Yang, Fu-San Chen and Ying-Shun Zhu. The field measurement and data collection were performed by Jian-Xin Zhou and Ya-Feng, Wu. The analysis was performed by Xian-Jian Sun and Chuang Shen. The first draft of the manuscript was written by Mei Yang, and all authors commented on previous versions of the manuscript. All authors read and approved the final manuscript.

Data availability The data that support the findings of this study are openly available in Science Data Bank at https://cstr.cn/31253.11.sciencedb.34304 and https://www.doi.org/10.57760/sciencedb.34304.

Declarations

Conflict of interest The authors declare that they have no conflict of interest.

References

1. CEPC Accelerator Study Group, CEPC conceptual design report volume I (Accelerator) 2018. IHEP-CEPC-DR-2018-01. https://doi.org/10.48550/arXiv.1809.00285
2. CEPC Study Group, CEPC technical design report: accelerator. Radiat. Detect. Technol. Methods **8**, 1–1105 (2024). https://doi.org/10.1007/s41605-024-00463-y
3. D. Wang, J. Gao, M.Q. Ruan et al., CEPC cost model study and circumference optimization. J. Instrum. **17**(10), P10018 (2022). https://doi.org/10.1088/1748-0221/17/10/P10018
4. Y.W. Wang, F. Su, S. Bai et al., Lattice design for the CEPC double ring scheme. Int. J. Mod. Phys. A **33**(2), 184001 (2018). https://doi.org/10.1142/S0217751X18400018
5. Y.S. Zhu, X.C. Yang, R. Liang et al., Final focus superconducting magnets for CEPC. IEEE T. Appl. Supercon. **30**, 4002105 (2020). https://doi.org/10.1109/TASC.2020.2973110
6. C. Shen, Y.S. Zhu, F.S. Chen, Analytical computation of magnetic field in coil-dominated superconducting quadrupole magnets based on racetrack coils. Nucl. Sci. Tech. **35**, 76 (2024). https://doi.org/10.1007/s41365-024-01437-x
7. J.Y. Zhai, D.J. Gong, H.J. Zheng et al., Design of CEPC superconducting RF system. Int. J. Mod. Phys. A **34**(10), 1940006 (2019). https://doi.org/10.1142/S0217751X19400062
8. H.J. Zheng, J. Gao, J.Y. Zhai et al., RF design of 650-MHz 2-cell cavity for CEPC. Nucl. Sci. Tech. **30**, 155 (2019). https://doi.org/10.1007/s41365-019-0671-6
9. Y.W. Wang, S. Bai, C.H. Yu et al., The energy sawtooth effects in the partial double ring scheme of CEPC. Int. J. Mod. Phys. A **34**(13n14), 1940008 (2019). https://doi.org/10.1142/S0217751X19400086
10. W.B. Liu, Y. Zhang, T.M. Xin et al., Advancements in the development of beam dynamics software APES for CEPC. Proc. IPAC'24, 1018–1021.https://doi.org/10.18429/JACoW-IPAC2024-TUPC11
11. R. Bailey, B. Balhan, C. Bovet et al., Synchrotron radiation effects at LEP. CERN-SL-98-046-OP (1998). https://cds.cern.ch/record/360833
12. M. Yang, F.S. Chen, X.J. Sun et al., Development of the CEPC Collider prototype magnets. Int. J. Mod. Phys. A **36**(22), 2142009 (2021). https://doi.org/10.1142/S0217751X21420094
13. M. Yang, F.S. Chen, W. Chen et al. CEPC collider and booster magnets. 62th ICFA ABDW on High Luminosity Circular e + e- Colliders (eeFACT'18), Hong Kong, China, 24-27 September 2018. JACOW Publishing, Geneva, Switzerland, 247–250 (2019) https://doi.org/10.18429/JACoW-eeFACT2018-WE0BB05
14. M. Yang, F.S. Chen, Y.F. Wu et al., Development of short prototype of dual aperture quadrupole magnet for CEPC ring. Nucl. Sci. Tech. **34**, 103 (2023). https://doi.org/10.1007/s41365-023-01255-7
15. The FCC Collaboration, FCC-ee:the lepton collider: future circular collider conceptual design report volume 2. Eur. Phys. J. Spec. Top. **228**, 261–623 (2019). https://doi.org/10.1140/epjst/e2019-900045-4
16. A. Milanese, Efficient twin aperture magnets for the future circular e^+/e^- collider. Phys. Rev. Accel. Beams. **19**, 112401 (2016). https://doi.org/10.1103/PhysRevAccelBeams.19.112401
17. A. Milanese, M. Bohdanowicz, Twin aperture bending magnets and quadrupoles for FCC-ee. IEEE T. Appl. Supercond. **28**(3), 4000904 (2018). https://doi.org/10.1109/TASC.2017.2772840
18. A. Milanese, J. Bauche, C. Petron, Magnetic measurements of the first short models of twin aperture magnets for FCC-ee. IEEE T. Appl. Supercond. **30**(4), 4003905 (2020). https://doi.org/10.1103/PhysRevAccelBeams.19.112401
19. European Organization for Nuclear Research. LEP design report: Vol II the LEP main ring. CERN-LEP/84-01, June (1984)
20. J.P. Gourber, L. Resegotti, Implications of the low field levels in the LEP magnets. IEEE T. Nucl. Sci. **26**(3), 3185–3187 (1979). https://doi.org/10.1109/TNS.1979.4329978
21. C. Carli, L. Fiscarelli, and D. Schoerling, Considerations on the effect of magnet yoke dilution on remanent field at ELENA. 8th Int. Particle Accelerator Conf. (IPAC'17), Copenhagen, Denmark, 14–19. JACOW, Geneva, Switzerland, 4299–4302 (2017) https://doi.org/10.18429/JACoW-IPAC2017-THPIK092
22. Dassault System. Opera: Electromagnetic and electromechanical simulation (2021). https://www.3ds.com/products/simulia/ opera
23. A.K. Jain, Measurements of field quality using harmonic coils. US Particle Accelerator School on Superconducting Accelerator Magnets (2001). https://cds.cern.ch/record/1246517/files/p175.pdf
24. N.O. Strelnikov, I.B. Vasserman, Earth's field effect on magnetic performance of horizontally and vertically polarizing undulators. Phys. Rev. ST Accel. Beams **17**(6), 062401 (2014). https://doi.org/10.1103/PhysRevSTAB.17.06240
25. Z. Zhang, F.S. Chen,B. Chen et al., The magnetic measurement for low magnetic field stability of dipole magnet for CEPC. 6th Int. Particle Accelerator Conf. (IPAC'15), Richmond, VA, USA, May 3–8, 2015. JACOW, Geneva, Switzerland, 2917–2920 (2015). https://doi.org/10.18429/JACoW-IPAC2015-WEPMN003
26. J.J. Zhao, Z.S. Zhao, *Particle Accelerator Technology* (Higher Education Press, Beijing, 2006)
27. P.C. Kohnke, Ansys. Finite element systems: a handbook. Berlin, Heidelberg: Springer Berlin Heidelberg (1982). http://www.ansys.com
28. W. Kang, J.X. Zhou, Y.H. Li et al., Research and development of the high precision low field dipole magnet for CEPC Booster. J. Instrum. **10**(02), P02006 (2024). https://doi.org/10.1088/1748-0221/19/02/P02006
29. S. Sanfilippo, Hall probes: physics and application to magnetometry. https://doi.org/10.48550/arXiv.1103.1271
30. J.T. Tanabe, Iron dominated electromagnets: design, fabrication, assembly and measurements. World Scientific (2005). https://www.slac.stanford.edu/pubs/slacreports/reports16/slac-r-754.pdf
31. A.M. Jain, Harmonic coils. (1998). https://cds.cern.ch/record/1246517/files/p175.pdf
32. S. Russenschuck, *Field Computation for Accelerator Magnets: Analytical and Numerical Methods for Electromagnetic Design and Optimization* (John Wiley & Sons, New Jersey, 2011)
33. J.X. Zhou, W. Kang, S. Li et al., Research on measurement of integral field uniformity of CSNS corrector magnets. High Power Laser Part. Beams **31**, 115105 (2019). https://doi.org/10.11884/HPLPB201931.190028
34. L. Dupré, J. Melkebeek, Electromagnetic hysteresis modelling: from material science to finite element analysis of devices. Int. Compumag. Soc. Newsl. **10**(3), 4–15 (2003). http://hdl.handle.net/1854/LU-212428
35. J.R. Anglada, P. Arpaia, M. Buzio et al., Characterization of magnetic steels for the FCC-ee magnet prototypes. In *2020 IEEE*

International Instrumentation and Measurement Technology Conference (I2MTC). IEEE, pp. 1–6. (2020) https://doi.org/10.1109/I2MTC43012.2020.9129153

36. J. Gourber, L. Resegotti, Implications of the low field levels in the LEP magnets. IEEE T. Nucl. Sci. **26**, 3185–3187 (1979). https://doi.org/10.1109/TNS.1979.4329978